Towards a CFD Model for Prediction of Wind Turbine Power Losses due to Icing in Cold Climate

Marie Cecilie Pedersen[1,2]*, Henrik Sørensen[1]

ISROMAC 2016

International Symposium on Transport Phenomena and Dynamics of Rotating Machinery

Hawaii, Honolulu

April 10-15, 2016

Abstract

Icing induced power losses is an important issue when operating wind turbines in cold climate. This paper presents a concept of modelling ice accretion on wind turbines using Computational Fluid Dynamics (CFD). The modelling concept works towards unifying the processes of modelling ice accretion and the aerodynamic analysis of the iced object into one CFD-based icing model. Modelling of icing and obtaining ice shapes in combination with mesh update by surface boundary displacement was demonstrated in the paper. It has been done by expressing in-cloud icing in CFD by an Eulerian multiphase model, implementing an icing module into the CFD solution and finally by surface boundary displacement also included in the CFD solution. The model has been developed using ANSYS-FLUENT and user-defined functions. The naca profile, NACA64618, has been used to illustrate the functionality of the model. Running ice accretion for different meteorological boundary conditions has illustrated the capabilities of the model and the generated ice shapes showed agreement with the literature.

Keywords

Ice accretion — Surface boundary displacement — CFD

[1] *Department of Energy Technology, Aalborg University, Aalborg, Denmark*

[2] *Operation and Site Technology, Wind R&D, Vattenfall A/S, Kolding, Denmark*

*__Corresponding author__: mcpe@et.aau.dk, marie.ceciliepedersen@vattenfall.com

INTRODUCTION

Wind power in cold climate has become more common especially in Nordic countries, such as Sweden, Finland, Norway and Canada. The current total installed capacity of wind power in cold climate is approximately 70 GW, which is expected to increase up to 70% towards the end of 2017 [1]. Cold climate areas are defined by experiencing temperatures below the operating limits of standard wind turbines and by the presence of icing events. Cold climate is attractive for wind energy extraction due to the low air density, remote location and most likely sparse population. Nevertheless, producing electricity in cold climate regions is challenging due to icing related risks, such as ice being shed from the turbine blade, blade fatigue due to additional ice load and finally production losses due to icing. In remote cold climate areas the most severe risk is the production losses, which can have tremendous impact on the profitability of a wind farm.

Production losses in cold climate happens during atmospheric icing, by the impact of moisture on a surface at temperatures below 0^{o}C resulting in ice accretion. The interest of this work is periods where the conditions are in favour of building up, which is called meteorological icing. Ice building up during meteorological icing is referred to as *ice accretion*. Opposite, periods where the accreted ice remains on the structure is called instrumental icing [2]. Atmospheric icing can be divided into 3 main categories; in-cloud icing, freezing rain and wet snow icing. During in-cloud icing super-cooled droplets are present in a cloud or fog at cold temperatures resulting in the formation of hard rime, soft rime or glaze ice depending on the temperature [2]. In this work in-cloud icing at cold temperatures and thereby the formation of rime ice has been modelled.

Modelling of icing has been studied for power lines, within aeronautics, for structures and objects and more recently also for wind turbines. Within wind power, the aeronautic icing models such as Messinger's thermodynamic model from 1953 [3] and the panel based code LEWICE [4] have been widely used and accepted. Also the CFD code FENSAP-ICE originally developed for the aircraft industry has been applied to wind turbine applications, as seen in [5] where performance degradation and power losses were studied. Other icing models highly used within wind power are the empirical tuned cylinder based model by Makkonen [6] [2] and the panel based code TURBICE designed for de-icing applications [7]. Recent studies by [8] has managed to advancing Makkonen's cylinder based model to be more representative for a wind turbine. Common for LEWICE, TURBICE and Makkonen's cylinder based model is that the codes generate ice shapes. To study aerodynamic response of wind turbines during or after icing conditions the ice shape could be obtained of one of the latter mentioned methods followed by the use of CFD to study the aerodynamic changes. This was seen in [9] where LEWICE was used to generate icing shapes for a variation of meteorological conditions followed by a aerodynamic study using ANSYS-FLUENT. Thus, obtaining the ice shape was separated from the aerodynamic analysis, which was also seen in recent studies by [10]. In [11] and [12] the ice shapes

were obtained from experiments followed by CFD analysis of the aerodynamic response. The objectives of this work is to develop a concept, which unifies the ice accretion process and the aerodynamic analysis into one CFD-based ice accretion model.

1. METHODS

The aim of the ice accretion model is to mimic an icing event in the best possible way by employing a CFD-based frame and to make the model as generic as possible. The Eulerian multiphase flow model has been used to imitate icing conditions in various CFD-based icing models. This is seen by the commercial code FENSAP-ICE, originally developed for the aircraft industry [13], which has recently been applied for wind turbine applications [14] and [5]. In other studies using ANSYS-FLUENT the Eulerian multiphase flow model has also been applied to imitate in-cloud icing conditions for ice accretion [15] and [16]. From the droplet solution of the Eulerian multiphase model, the variables of velocity, volume fractions, density and temperature for the phases will be available everywhere in the computational domain at any time.

The ice accretion model used in this study was inspired by Messiger's model [3], which has been applied for other CFD icing applications especially for aircraft purposes [13]. Nevertheless, the model in combination with an Eulerian multiphase flow model has also shown reasonable results and applications for wind turbines [10] and [14]. The modelling approach is structured as illustrated by Figure 1, which consists of 3 main modules; 1) obtain multiphase flow solution, 2) ice accretion model and 3) surface boundary displacement. The ice accretion model and the surface boundary displacement is included in the ANSYS-FLUENT solver by using user-defined functions. Unique for the proposed modelling structure in Figure 1 is that the three modules are updated every time-step adding a high accuracy to the model. Updating the multiphase flow solution after every surface boundary displacement ensures the changes in geometry to be reflected in the flow solution. Other icing models, such as FENSAP-ICE [13] either uses an initial particle flow solution over the entire ice accretion time or uses a so-called quasi-steady approach, where the droplet solution are updated a given number of times during the ice accretion time [13]. Since the droplet solution and collection efficiency (β) will change over time, see example in Figure 2, it is found necessary to update the Eulerian flow solution every time-step to ensure a reliable representation of the actual multiphase flow of air and particles at the given time of the ice accretion period. Figure 2 shows the change in collection efficiency (β, Equation 4) over time and the corresponding shape of the airfoil exposed to icing over time.

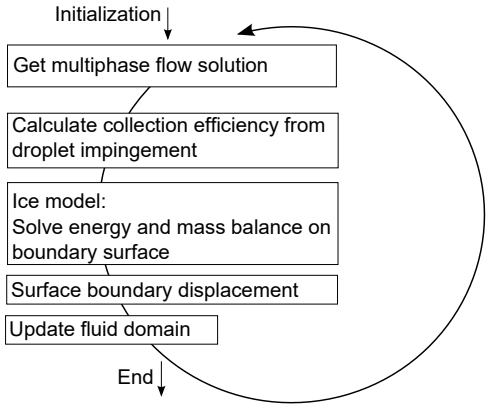

Figure 1. Modelling structure.

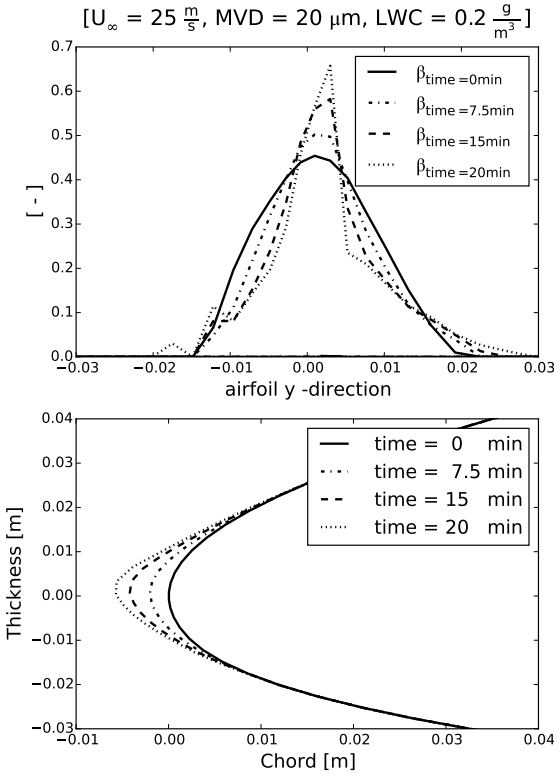

Figure 2. Top: variation in collection efficiency (β) over 20 minutes of ice accretion. Bottom: corresponding ice shapes during 20 minutes of ice accretion.

Multiphase flow modelling The Eulerian description of a multiphase flow involves the concept of phasic volume fractions, α_q, which describes the space occupied by each phase. The laws of conservation of mass and momentum are satisfied by each phase individually [17]. The sum of all phases equals to one

$$\sum_{q=1}^{n} \alpha_q = 1 \tag{1}$$

The volume fraction of each phase of the two-phase flow is solved by the continuity equation, shown here for phase q

$$\left(\frac{\partial}{\partial t}(\alpha_q \rho_q) + \nabla \cdot (\alpha_q \rho_q \vec{v}_q) \right) = \sum_{p=1}^{n} \left(\dot{m}_{pq} - \dot{m}_{qp} \right) + S_q \tag{2}$$

where $\vec{v}_q$ is the velocity vector of phase q and $m_{pq,qp}$ characterize the mass transfer between the p^{th} and q^{th}phase. There is no mass exchange between the phases and no mass source are added for the phases, leaving the right hand side of Equation 2 to zero. The solution of Equation 2 for the secondary phase together with the conditions of Equation 1 allows for the calculation of the primary-phase volume fraction. The conservation of momentum for the fluid phase q is given as

$$\begin{aligned}\frac{\partial}{\partial t}(\alpha_q\rho_q\vec{v}_q) + \nabla\cdot(\alpha_q\rho_q\vec{v}_q\vec{v}_q) &= -\alpha_q\Delta p \\ &+ \Delta\cdot\bar{\bar{\tau}}_q + \alpha_q\rho_q\vec{g}+ \\ &+ \sum_{p=1}^{n}(K_{pq}(\vec{v}_p - \vec{v}_q)) \\ &+ (\vec{F}_q + \vec{F}_{\text{lift},q} + \vec{F}_{\text{wl},q} + \vec{F}_{\text{td},q}) \qquad (3)\end{aligned}$$

where $\vec{g}$ is the acceleration due to gravity, and K_{pq} is the momentum exchange coefficient between the phases, Δp, $\bar{\bar{\tau}}_q$, $\vec{F}_q$, $\vec{F}_{\text{lift},q}$, $\vec{F}_{\text{wl},q}$, $\vec{F}_{\text{td},q}$ are the pressure gradient, stress-strain tensor, external body force, lift force, wall lubrication force and the turbulent dispersion force respectively. The energy conservation for the Eulerian multiphase model is solved by a separate enthalpy equation for each phase of the flow [17]. The k-ω SST turbulence is applied to the multiphase flow based on a preliminary study [16].

Ice accretion model For the simulation of ice accretion only rime ice has been considered. Figure 3 illustrates the mass balance of rime ice accretion on the surface boundary of an object, where m_{imp} is the mass of droplets impinging on the object, m_{subl} is sublimation of ice mass from solid to vapor and m_{ice} is the accumulated ice mass. It is assumed that all mass which impinge on the body will freeze instantaneously and turn into ice, see Equation 5. In the model, the accreted ice mass becomes part of the object by applying a surface boundary displacement algorithm. Enclosing the accumulated mass of ice into the object geometry allows for studying the aerodynamic changes due to ice accretion.

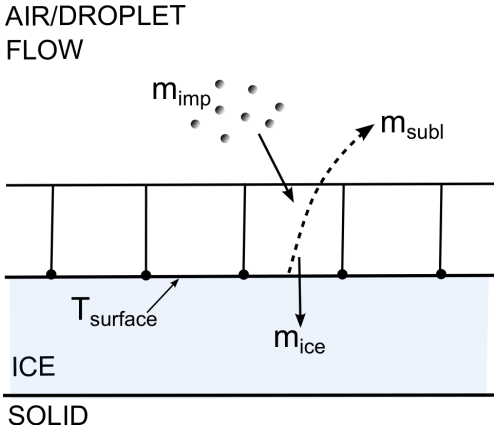

Figure 3. Mass balance of rime ice accretion on surface boundary.

The mass of accumulated ice m_{ice}, is found instantaneously over time based on the collection efficiency (β)

$$\beta = \frac{\alpha_{\mathbf{n}}(\mathbf{u}_d\cdot\mathbf{n})}{U_\infty} \qquad (4)$$

$$m_{imp} \approx m_{ice} = \beta U_\infty \text{LWC} \qquad (5)$$

where α_n is the normalised droplet volume fraction $\left(\frac{\alpha_{d,imp}}{\alpha_\infty}\right)$, u_d is the droplet impact velocity, $\mathbf{n}$ is the unit surface normal and U_∞ is the free-stream velocity. The normalised velocity $u_{\mathbf{n}}$ is given as $\left(\frac{\mathbf{u}_d}{u_\infty}\right)$. Thus the amount of accumulated ice mass is a function of the collection efficiency, the liquid water content in the cloud and the free-stream velocity.

Surface boundary displacement The mass of instantaneously accumulated ice (m_{ice}) initiates the surface boundary displacement. The surface boundary displacement is constructed around the Dynamic-mesh package available in ANSYS-FLUENT [17], from where the DEFINE_GRID_MOTION macro has been used. The macro is transient and by an iterative process the node point of the surface can be updated. This means, that the mesh will be updated at every time step. The mesh is updated by a node displacement vector $\vec{v}_{n,i}$

$$\vec{v}_{n,i} = \frac{m_{ice}}{\rho_{ice}}\mathbf{n} \qquad (6)$$

where ρ_{ice} is the density of ice. The node displacement vector gives a set of coordinates of the new location of the node. The process is obtained by a face-looping and node-looping approach as illustrated in Figure 4. The instantaneously mass

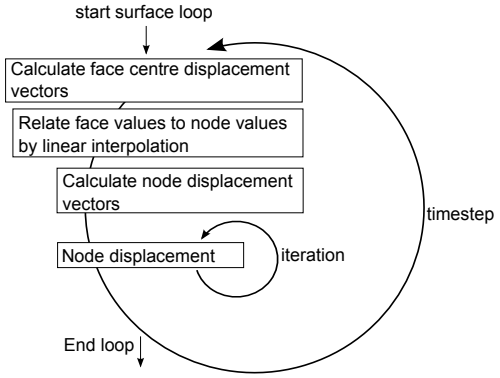

Figure 4. Surface boundary displacement.

of ice and the boundary displacement vector is calculated at each face (f) of the surface boundary as illustrated in Figure 5. By linear interpolation the contribution from the node neighbouring faces (f_L, f_R) to the node displacement vector at node i (n,i) is enabled. The node positions are updated according to the following expression

$$p_{n,i}^{t+\Delta t} = p_{n,i}^{t} + v_{n,i}^{t}\Delta t \qquad (7)$$

where $p_{n,i}$ is the current node positions, t is the current time and Δt the time step.

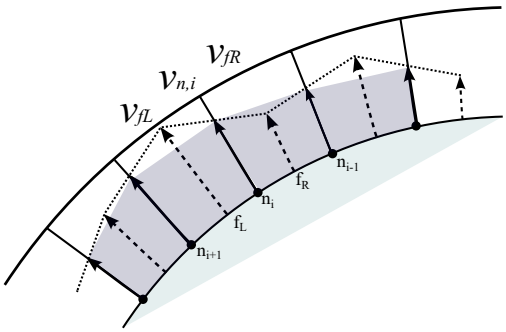

Figure 5. Surface boundary displacement by surface displacement vectors.

1.1 Model Set-up

A set of simulations have been carried out to illustrate the capabilities of the CFD icing model. The NACA64618 profile with a sharp trailing edge has been used for the simulation in a computational domain consisting of 4050 cells, in a C-grid shape, as seen in Figure 6. The NACA64618 profile was used, since it is part of the 5MW virtual NREL wind turbine also used for other icing studies [5] and [9]. The model inputs are presented in the following by specifying the conditions for the secondary phase (the super-cooled droplets) and for the primary phase (the airflow).

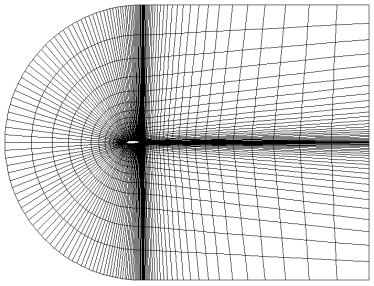

Figure 6. Computational domain.

Secondary phase inputs From the liquid water content and density the volume fraction of the secondary phase have been specified as

$$\alpha_d = \frac{\text{LWC}}{\rho_d} \tag{8}$$

where ρ_d is the density of the super-cooled droplets. Simulations of ice accretion have been carried out for the different cases of secondary phase settings presented in Table 1.

Meteorological inputs The meteorological conditions of the rime ice events are inspired by [9] and presented in Table 2. The droplet size allows for a one-way coupling to exist between the airflow and the droplets.

Surface roughness The surface roughness is a significant parameter to include in an ice model since it determines the transition location of the airflow from laminar to turbulent over the rough surface. The sand grain roughness depends

Table 1. Table of CFD model inputs: secondary phase.

Secondary phase conditions		
LWC $\frac{g}{m^3}$	MVD μm	α_d -
0.05	8, 12, 16, 20	$7.69 \cdot 10^{-8}$
0.1	8, 12, 16, 20	$1.54 \cdot 10^{-7}$
0.15	8, 12, 16, 20	$2.31 \cdot 10^{-7}$
0.20	8, 12, 16, 20	$3.08 \cdot 10^{-7}$
0.25	8, 12, 16, 20	$3.85 \cdot 10^{-7}$

Table 2. Table of CFD model inputs: meteorological inputs.

Meteorological boundary conditions			
Phases:	primary (airflow)	dispersed (droplets)	
U_∞	25	25	$\frac{m}{s}$
T_∞	-10	-10	^{o}C

on the actual icing condition seen by the iced object. A way to take roughness into account is by employing a sand grain roughness (K_s) [7] and [18] based on empirical roughness parameters as

$$K_s = \left(\frac{k_s^*}{k_{sb,\text{LWC}}^*}\right)\left(\frac{k_s^*}{k_{sb,T_\infty}^*}\right)\left(\frac{k_s^*}{k_{sb,U_\infty}^*}\right)\left(\frac{k_s^*}{k_{sb,\text{MVD}}^*}\right)k_{sb}^* c \tag{9}$$

where c is the cord length in meters. The empirical roughness parameters are defined as follows

$$\begin{aligned}
\left(\frac{k_s^*}{k_{sb,\text{LWC}}^*}\right) &= (0.5714 + 0.2457(\text{LWC}) \\
&\quad + 1.2571(\text{LWC})^2) \\
\left(\frac{k_s^*}{k_{sb,T_\infty}^*}\right) &= (0.047T_\infty - 11.27) \\
\left(\frac{k_s^*}{k_{sb,U_\infty}^*}\right) &= (0.4286 + 0.0044139U_\infty) \\
\left(\frac{k_s^*}{k_{sb,\text{MVD}}^*}\right) &= \left(\frac{1, \quad \text{MVD} \leq 20}{1.667 - 0.0333(\text{MVD}),\ \text{MVD} > 20}\right) \\
k_{sB}^* &= (0.001177)
\end{aligned}$$

During ice accretion the sand-grain roughness will change affecting the transitions area and flow field at the boundary of the iced object. In [7] the time dependence of the surface roughness height is taken into account by multiplying by a factor depending on the freezing fraction (f), the fraction of particles which actually freeze at impact and the number of ice layers simulated. The freezing fraction is a number between 0-1, where 1 correspond to rime ice and $0 < f > 1$ is glaze ice conditions, [19]. For f close to or equal to 1 the sand

grain roughness is multiplied with 1 as soon as a reasonable rime ice layer is obtained. Thus, since only rime ice accretion is simulated in this study it is found reasonable to apply a constant sand-grain roughness based on Equation 9 from time equal to zero, even though this will enhance the ice accretion at the initial stage.

2. RESULTS AND DISCUSSION

The focus of this study has been on developing and testing the functionality of the presented CFD ice accretion model on the NACA64618 airfoil. The generated ice shapes have been compared to ice shapes presented in the work by Etemaddar et al. 2014 [9], where ice accretion has been simulated on the NACA64618 airfoil using the panel-based code LEWICE [4]. From [9] it was shown, that increasing LWC would increase ice accretion, especially in the direction of the chord. Likewise, increasing MVD would increase ice accretion but more severe along the thickness of the airfoil.

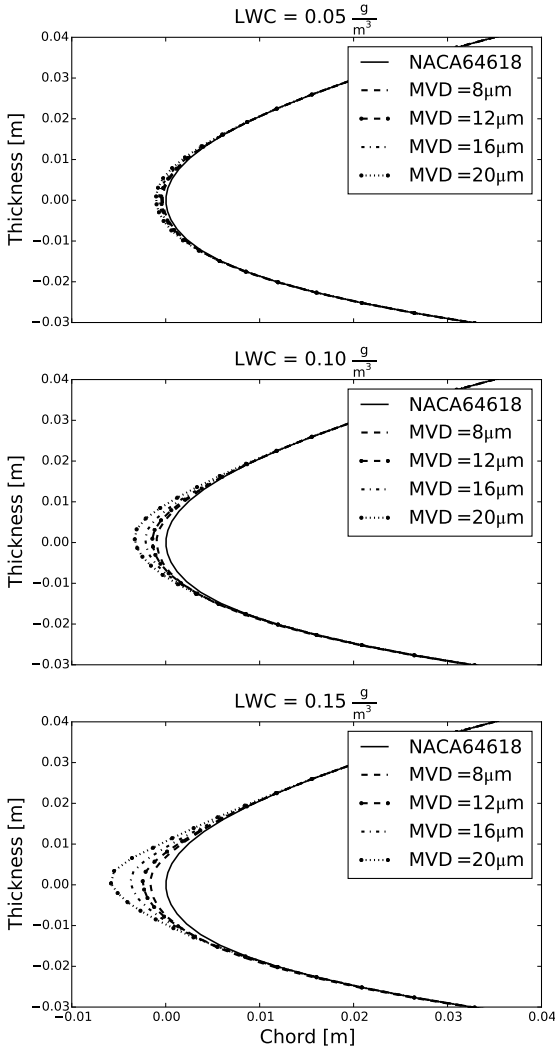

Figure 7. Generated ice shapes after 20 minutes of ice accretion using surface boundary displacement for U_∞ = 25 $\frac{m}{s}$, T_∞ = -10°C and LWC of 0.05 $\frac{g}{m^3}$, 0.10 $\frac{g}{m^3}$ and 0.15 $\frac{g}{m^3}$.

In this study, ice accretion has been simulated for 20 minutes with a time-step size of 0.01 second for all cases of secondary phase settings presented in Table 1 with the meteorological boundary conditions given in Table 2. Furthermore a constant density of ice of 650 $\frac{kg}{m^3}$ has been used an angle of attack of 0°. The generated ice shapes is seen for the cases of LWC of 0.05 $\frac{g}{m^3}$, 0.10 $\frac{g}{m^3}$ and 0.15 $\frac{g}{m^3}$ in Figure 7 for cases with LWC of 0.20 $\frac{g}{m^3}$ and 0.25 $\frac{g}{m^3}$ in Figure 8.

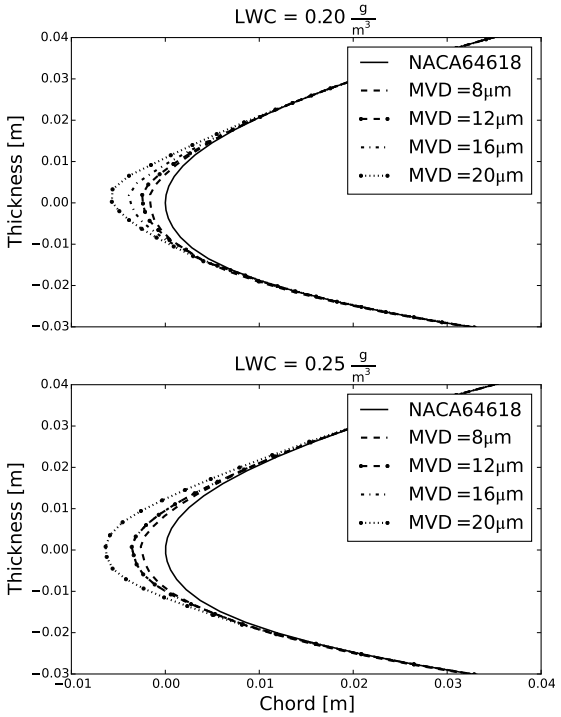

Figure 8. Generated ice shapes after 20 minutes of ice accretion using surface boundary displacement for U_∞ = 25 $\frac{m}{s}$, T_∞ = -10°C and LWC of 0.20 $\frac{g}{m^3}$ and 0.25 $\frac{g}{m^3}$.

Figure 7 and 8 illustrate how the total amount of ice accretion increased with an increasing LWC. Furthermore, the figures illustrates that increasing MVD will result in more ice accretion, which was most severe for the high numbers of LWC. This can be seen in Figure 8. The results from the simulations was in agreement with the conclusions regarding LWC and MVD found in [9] and [20].

2.1 Conclusions

From the study a promising concept towards a complete CFD model for prediction of wind turbine power losses due to icing in cold climate was established. The study has illustrated that it was possible to unify the ice accretion process with the aerodynamic analysis in one CFD ice accretion model. The concept has demonstrated the ability to model rime ice accretion and perform surface boundary displacement per time step for an icing period of 20 minutes. Furthermore, the simulated ice accretion cases showed agreement with the literature and the model was able to include the influence of droplet variation and variation in of the liquid water content.

Future work is to extend the icing time and include varying meteorological input conditions and finally to compare the model with site-measurements or data from a climatic wind tunnel, as seen by [21]. Furthermore, changes in lift and draft forces for a variation of angle of attacks should be studied.

ACKNOWLEDGMENTS

Marie Cecilie Pedersen would like to thank Vattenfall Vindkraft A/S for hosting and partly granting the Industrial Phd program and the *Innovation Fund Denmark* from the Danish Ministry of Higher education and Science for partly granting the program.

REFERENCES

[1] Timo Wallenius. Special Theme: Cold Climate Turbines("CCTs"). *BTM World Market Update, BTM-Consult*, pages 29–42, 2013.

[2] iso. Athmospheric Icing on strutures, ISO 12494:2001(E). Technical report, ISO, Geneva, Switzerland, 2001.

[3] Bernard L Messinger. Equilibrium Temperature of an Unheated Icing Surface as a Function of Air Speed. *Journal of the Aeronautical Sciences (Institute of the Aeronautical Sciences)*, 20(1):29–42, 1953.

[4] William Wright. User's Manual for LEWICE Version 3.2. Technical report, NASA, National Aeronautics and Space Administration, Glenn Research Center, Cleveland, Ohio, USA, 2008.

[5] Thomas Reid, Guido Baruzzi, Isik Ozcer, David Switchenko, and Wagdi Habashi. FENSAP-ICE Simulation of Icing on Wind Turbine Blades, Part 1: Performance Degradation. In *51st AIAA Aerospace Sciences Meeting including the New Horizons Forum and Aerospace Exposition 07-10 January 2013, Grapevine (Dallas Ft. Worth Region), Texas*, 2013.

[6] Lasse Makkonen. Models for the Growth of Rime, Glaze, Icicles and Wet Snow on Structures. *Philosophical Transactions: Mathematical, Physical and Engineering Sciences*, 358(1776):2913–2939, 2000.

[7] Lasse Makkonen, Timo Laakso, Mauri Marjaniemi, and Karen Finstad. Modelling and prevention of ice accretion on wind turbines. *Wind Engineering*, 25(1):3–21, 2001.

[8] Neil Davis. Icing Impacts on Wind Energy Production. *PhD diss., Vestas Wind Systems A/S and The Technical University of Denmark, DTU Wind Energy*, 2014.

[9] M. Etemaddar, M. O. L. Hansen, and T. Moan. Wind turbine aerodynamic response under atmospheric icing conditions. *Wind Energy*, 17(2):241–265, 2014.

[10] M Ali and N Sankar Lakshmi. In-Cloud Ice Accretion Modeling on Wind Turbine Blades Using Extended Messinger Model. In *13th International Energy Conversion Engineering Conference*, 2015.

[11] Fernando Villalpando, Marcelo Reggio, and Adrian Ilinca. Numerical study of flow around iced wind turbine airfoil. *Engineering Applications of Computational Fluid Mechanics*, 6(1):39–45, 2012.

[12] X Chi, Bin Zhu, T.I.P Shih, H.E. Addy, and Y.K. Choo. CFD analysis of the aerodynamics of a business-jet airfoil with leading-edge ice accretion. *AIAA Paper*, 560, 2004.

[13] NTI. User Manual FENSAP-ICE, Version 2012 release 1.1. Technical report, Newmerical Technologies International, Montreal, Quebec, Canada, 2012. Manual.

[14] David Switchenko, Wagdi G. Habashi, Guido Baruzzi, and Isik Ozcer. FENSAP-ICE Simulation of Complex Wind Turbine Icing Events, and Comparison to Observed Performance Data. In *32nd ASME Wind Energy Symposium*, 2014.

[15] Sutikno Wirogo and Shashidhar Srirambhatla. An Eulerian Method to Calculate the Collection Efficiency on Two and Three Dimensional Bodies. *AIAA paper*, 1073, 2003.

[16] Mare Cecilie Pedersen and Chungen Yin. Preliminary modelling study of ice accretion on wind turbines. *Energy Procedia*, 2014.

[17] ANSYS Inc. ANSYS Fluent Theory Guide. Technical Report Relaese 15.0, ANSYS, November 2013.

[18] Jaiwon Shin and Brian Berkowitz. Prediction of ice shapes and their effect on airfoil drag. *Journal of aircraft*, 31(2):263–270, 1994.

[19] Lorenzo Battisti. *Wind Turbines in Cold Climate*. Springer, Springer International Publishing Switzerland 2015, 1 edition, 2015.

[20] Matthew C Homola, Muhammad S Virk, Tomas Wallenius, Per J Nicklasson, and Per A Sundsbø. Effect of atmospheric temperature and droplet size variation on ice accretion of wind turbine blades. *Journal of wind engineering and industrial aerodynamics*, 98(12):724–729, 2010.

[21] Peter M Blasco, Jose Palacios, and Sven Schmitz. Investigation of Wind Turbine Power Generation During Atmospheric Icing by Multi-Disciplinary Experimentation. In *33rd Wind Energy Symposium*, 2015.